SCIENTIFIC REPORTS

OPEN

C_{60} as fine fillers to improve poly(phenylene sulfide) electrical conductivity and mechanical property

Received: 16 January 2017
Accepted: 16 May 2017
Published online: 30 June 2017

Maliang Zhang, Xiaotian Wang, Yali Bai, Zhenhuan Li & Bowen Cheng

Electrical conductive poly(phenylene sulfide) (PPS)/fullerene (C_{60}) composites were prepared by 1-chlornaphthalene blending method, and the interface effects of C_{60} and PPS on PPS/C_{60} properties were characterized. C_{60} is an excellent nanofiller for PPS, and 2 wt% PPS/C_{60} composite displayed the optimal conductivity which achieved 1.67×10^{-2} S/cm. However, when C_{60} concentration reached 2 wt%, the breaking strength and tensile modulus of PPS/C_{60} fiber achieved maximum 290 MPa and 605 MPa, and those values were 7.72 and 11.2 times as that of pure PPS. The excellent conductive and mechanical properties of PPS/C_{60} were attributed to the heterogeneous nucleation of C_{60} during PPS crystallization, formation of a large number of covalent bond by main C_{60}-thiol adducts and minor C_{60}-ArCl alkylation between C_{60} outer surface and PPS matrix. At same time, PPS/C_{60} thermal properties were also investigated.

Fullerene/polymer composites have recently attracted considerable attention from the materials research community[1–3]. It has been shown that the incorporating fullerene or its derivatives into a polymer matrix could significantly improve its photovoltaic, electromechanical and thermomechanical properties[4,5]. The literature already identified several techniques to blend fullerene with polymers[3], and the properties of fullerene/polymer composites are closely related to the morphologies of the polymers formed during melt or solution processing[3,4]. Chemical functionalization of fullerenes is often performed to increase the miscibility of fullerenes with host polymers[6], but the chemical functionalization method makes fullerenes lost certain original precious properties, which resulted in chemical attachment of fullerenes to a polymer is not always the most effective method for getting high performance composite materials, despite a number of fullerene-attached polymers have been successfully synthesized in the past[7].

PPS is widely used in practice due to its excellent properties, such as chemical resistance, low coefficient of friction, mechanical behaviors, dimensional stability and electrical property[8–10]. To improve the performance of PPS, the nanofiller-reinforced composites require homogenous filler dispersion and good interfacial adhesion with the host matrix. Attaching functional groups onto the filler surface has been proven to be an effective approach to prepare polymer composites, and another effective method is wrapping fillers by organic molecules to provide the π-π stacking interactions between PPS matrix and nanofiller sidewalls. The conventional fillers included single-walled carbon nanotubes (SWCNTs)[11,12], inorganic fullerene-like tungsten disulfide (IF-WS_2)[13], SWCNT-IF-WS_2[14–16], functionalized SWCNTs and MWCNTs[17–20], nano particles of TiO_2, ZnO, CuO and SiC[21], nanoscale alumina particles[22], graphite[23], glass fiber[24], metal inorganic salt[25], nano-SiOx[26], carbon and fiber[27] *et al.* However, it has been recently shown that the properties of PPS based composites hardly increase at low nanofiller loadings (up to 1 wt%)[14,28,29]. Because of van der Waals attraction between C_{60} and their large surface area, C_{60} tend to form agglomerates during mixing with PPS by melt blending. Therefore, it is difficult to use the conventional method to disperse C_{60} in the PPS matrix.

Herein, C_{60} was selected as fillers to improve PPS electrical conductivity and mechanical property, and the influence of the 1-chloronaphthalene solution mixing method and subsequent melt process on filler dispersion, C_{60} interfacial adhesion with PPS matrix and composite properties were investigated to correlate the microscopic structure with macroscopic properties.

State Key Laboratory of Separation Membranes and Membrane Processes, School of Materials Science and Engineering, Tianjin Polytechnic University, 300160, Tianjin, China. Correspondence and requests for materials should be addressed to Z.L. (email: Zhenhuanli1975@aliyun.com) or B.C. (email: Bowen15@tjpu.edu.cn)

Experimental

Materials and reagents. C_{60} powder (>99.9 wt/wt purity) was purchased from Puyang Yongxin Fullerene Co., Ltd, and used as received. PPS (Mw~3.3×10^4, Mw/Mn~1.4×10^4, d25 °C~1.35 g/cm^3, Tg~90 °C, Tm~280 °C) was synthesized from Na_2S and 1,4-dichlorobenzene in N-methylpyrrole, and the end groups of synthesized PPS contained –SH and -PhCl. 1-chlornaphthalene (95%, Fluka) was purchased from J& K Chemical Co., Ltd and purified by distillation under reduced pressure before use.

Sample preparation. PPS (5 g) was dissolved in 100 ml of 1-chloronaphthalene at 205 °C under nitrogen atmosphere. After that, a certain amount of C_{60} ranging from 0.5 to 10 wt% were loaded into PPS/1-chloronaphthalene solution at 205 °C under mechanical agitation. PPS/C_{60} composites with 0.5 to 10 wt% nanofiller were obtained after removing 1-chloronaphthalene under vacuum condition. And then PPS and PPS/C_{60} composite fibers with diameters of 45~85 μm were prepared by melt spinning technology at 315 °C.

Characterization and Measurement. Fourier transform infrared spectroscopy (FT-IR) spectra were obtained using Bruker IFS66 at room temperature. Thermo gravimetric analyzer (TGA) analysis was carried out on a NETZSCH STA 409 TG analyzer, and the rate of temperature increase was at 10 °C/min. X-ray diffraction (XRD) data were obtained using an Elmer PHI-5600 instrument using a Mg Kα line as a radiation source and a D8 discover. The morphology of composites was characterized by a field emission scanning electron microscopy (FESEM, Hitachi 4800S, and Japans) and transmission electron micrographs (TEM, Hitachi H-7650 microscope). Differential scanning calorimetry (DSC) analysis was performed on a Perkin Elemer DSC-7 under nitrogen condition, and samples placed in aluminium pans were melted at 320 °C and kept at this temperature for 5 min to erase their thermal history. Subsequently, they were cooled from the melt to room temperature and then heated again up to 320 °C at a scan rate of 10 °C/min. From the DSC heating and cooling traces, peak melting temperature (T_m), heat of melting (ΔH_m), peak crystallization temperature (T_c) and heat of crystallize (ΔH_c) were obtained. The degree of crystallinity (X_c) was calculated from the following equation:

$$X_c(\%) = \frac{\Delta H_c}{\Delta H_f(1 - W_f)} \times 100\% \tag{1}$$

Where ΔH_c is the cold crystallization enthalpy from the DSC scan, W_f is the weight fraction of C_{60} in composites, and ΔH_f is the melting enthalpy of 100% crystallized PPS which was taken as 105 J/g[23].

Fiber diameter data were obtained using a KEYENCE VHX-1000 microscope at room temperature. The breaking strength (δ_t), breaking elongation (ε) and tensile modulus (MPa) were measured on single fiber strength tester (China LLY-06). Each sample was tested ten times to evaluate the average value. The breaking strength was calculated from the following equation:

$$\delta_t(MPa) = 4\frac{F_b}{\pi d^2} \times 10^{-6} \tag{2}$$

Where F_b is the maximum tension value, d is the fiber diameter. The breaking elongation was determined by the following equation:

$$\varepsilon(\%) = \frac{L - L_0}{L_0} \tag{3}$$

Where ε is the breaking elongation, L is the length of fiber elongation, L_0 is the initial length of the fiber before test. The fiber tensile modulus (E MPa) was determined by the following equation:

$$E = \frac{\delta_t}{\varepsilon} = \frac{4F_bL_0}{\pi d^2(L - L_0)} \times 10^{-4} \tag{4}$$

Electrical conductivity of samples was measured by the four-point probe method using a Scientific Equipment device with a spacing probe S = 0.2 cm equipped with a DC precision power source (Model LCS-02) and a digital microvoltmeter (Model DMV-001). The powder sample was filled into a test slot, then applying a pressure about 18 MPa. The electrical resistivity was calculated from the following equation:

$$\text{Electrical resistivity} = 2\,\pi S \times (W/S) \times D \times (V/I) \tag{5}$$

Where S is the distance of adjacent probe, W is the sample thickness, D is the position correction factor, V is the test voltage, I is the test current. Each sample has been tested ten times, and the electrical resistivity is the average value of 10 measurement. The electrical conductivity of samples was calculated through the following equations:

$$\text{Electrical conductivity} = 1/\text{Electrical resistivity} \tag{6}$$

Results

After C_{60} and PPS were dissolved in 1-chloronaphthalene, 1-chlornaphthalene evaporated under vacuum condition to obtain PPS/C_{60} composites, and the dispersion and alignment of C_{60} within the PPS matrix were characterized by TEM (Fig. 1). The dark and light areas correspond to nanofillers and PPS matix, respectively. The image of C_{60} showed a homogeneous size distribution with average diameter around 300 nm, which revealed C_{60} was easily

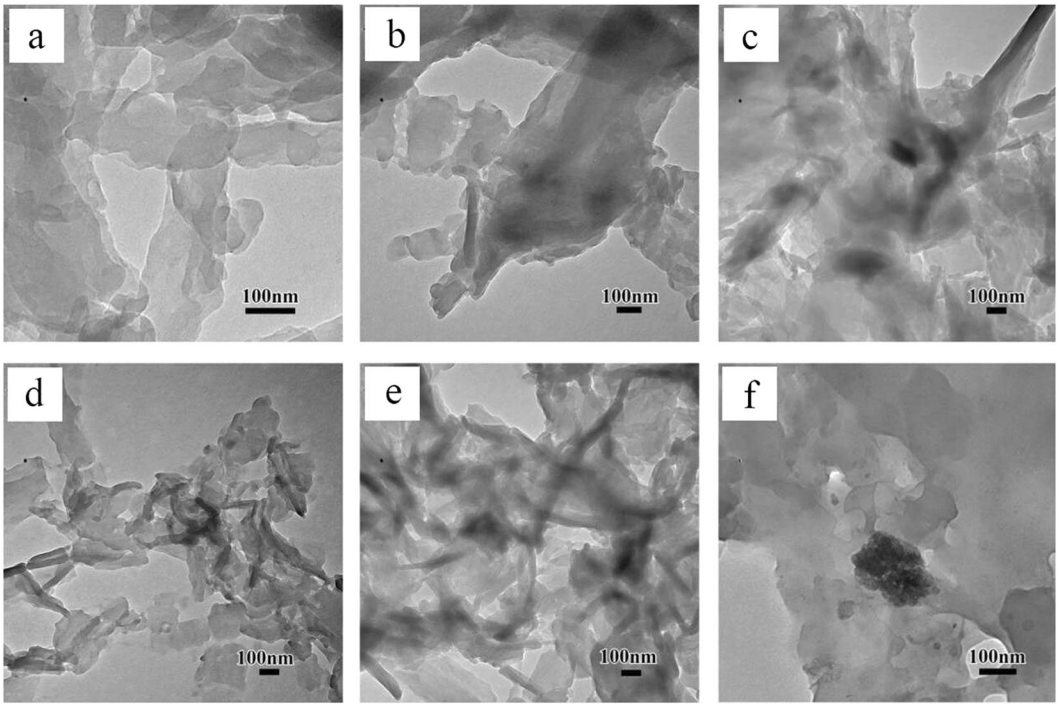

Figure 1. TEM micrographs of PPS/C_{60} powder with different weight fractions of C_{60} (**a**) Pure PPS; (**b**) 0.5 wt%; (**c**) 1 wt%; (**d**) 2 wt%; (**e**) 5 wt%; (**f**) 10 wt%.

agglomerated due to the strong van der Waals forces and intensive π-π stacking interactions among C_{60}. However, the micrograph of 0.5–2 wt% C_{60}/PPS composites indicated the aggregate C_{60} diameter decrease, and no voids or discontinuities are detected between the C_{60} outer surface and PPS matrix. The TEM micrograph of 0.5–2 wt% PPS/C_{60} fibers indicated that C_{60} was well dispersed into PPS matrix, however, when much more C_{60} was incorporated into PPS (such as 10 wt% PPS/C_{60}), C_{60} formed agglomerates inside the PPS matrix. TEM observation showed that C_{60} were wrapped in PPS or covered by PPS layer and the heterogeneous dispersed bright dots with dimensions from 150–350 nm in 5 wt% and 10 wt% PPS/C60 composites were detected, indicating good adhesion between C_{60} and PPS.

Figure 2 A shows the SEM micrograph of PPS as a blank example, and the SEM images of Fig. 2B,C,D indicated that almost no apparent C_{60} agglomerates were detected in 0.5 wt%, 1 wt% and 2 wt% PPS/C_{60} composites, due to C_{60} nanofillers further disaggregation within the polymer matrix during PPS/C_{60} melt-process. C_{60} nanofillers were randomly dispersed in the PPS matrix, occurring irregular crystal with dimensions from 20–50 nm when the content of C_{60} is less than 2 wt%. C_{60} nanofillers are difficult to disperse uniformly in PPS melt, therefore PPS can not well reinforced by C_{60} nanofillers in melt blending technology. However, C_{60} aggregates can be well dispersed in PPS matrix by solution blending method, in which the solvent plays a dual role in dispersing C_{60} and preventing C_{60} agglomeration. The heterogeneous dispersed bright dots with dimensions from 80–350 nm in 5 wt% and 10 wt% PPS/C_{60} composites were detected, which was attributed to C_{60} agglomerates. Similar results can also be found through the cross-sectional SEM images of the composites in Fig. 3. For PPS/C_{60}, 2 wt% C_{60} particles can be uniformly dispersed in PPS matrix, but further addition of 5 wt% C_{60} would cause the agglomeration of C_{60}, as can be seen in Fig. 3e and f.

X-ray diffraction patterns of PPS/C_{60} composites were displayed in Fig. 4. The two diffraction peaks at 19.2° and 20.8° are corresponding to the (110) and (200) crystalline planes of the orthorhombic structure of PPS[30]. And C_{60} shows characteristic peaks at $2\theta = 10.9°$, 17.2°, 20.8°, 21.8°, 28.2°, 30.8° and 32.7° arising from the (110), (220), (310), (220), (330), (420) and (330) crystalline planes of the orthorhombic unit cell, respectively[31]. The C_{60} agglomerate peaks were hardly visible in the diffractograms of 0.5–2wt% composites, which suggested that C_{60} was well dispersed in PPS matrix. After 5 wt% C_{60} was introduced into PPS, the serious C_{60} agglomerate was clearly observed, and the crystal characteristic peaks of C_{60} shifted to lower 2θ values bacause C_{60} aggregates result in PPS lattice distortion[32]. Moreover, composite peaks become broader with reduced intensity, indicating the structural order decline which induced by the incorporation of C_{60}. These observations are consistent with the behaviors of SWCNTs[33] and MWCNTs[34], where the local order of the polymer decreased after the grafting reaction.

As shown in Fig. 5, the main bands at 565, 615, 1218, 1470 and 1680 cm^{-1} are characteristic absorption peak of C_{60}[35]. The phenyl groups of PPS exhibited the absorption peaks at 1628 and 1405 cm^{-1}, and the two bands at 1100 and 623 cm^{-1} were attributed to aromatic C-S stretching vibrations. After PPS was reinforced by C_{60}, C_{60} characteristic absorption peaks at 565 and 1475 cm^{-1} band were still observed, which demonstrated the C_{60} successful incorporation into PPS matrix. However, C_{60} band at 1218 cm^{-1} disappeared and a new peak at 1010 cm^{-1} appeared, which implied the well C_{60} dispersion and C_{60}-S formation (Fig. 6)[36,37]. Solvent could help the tangled

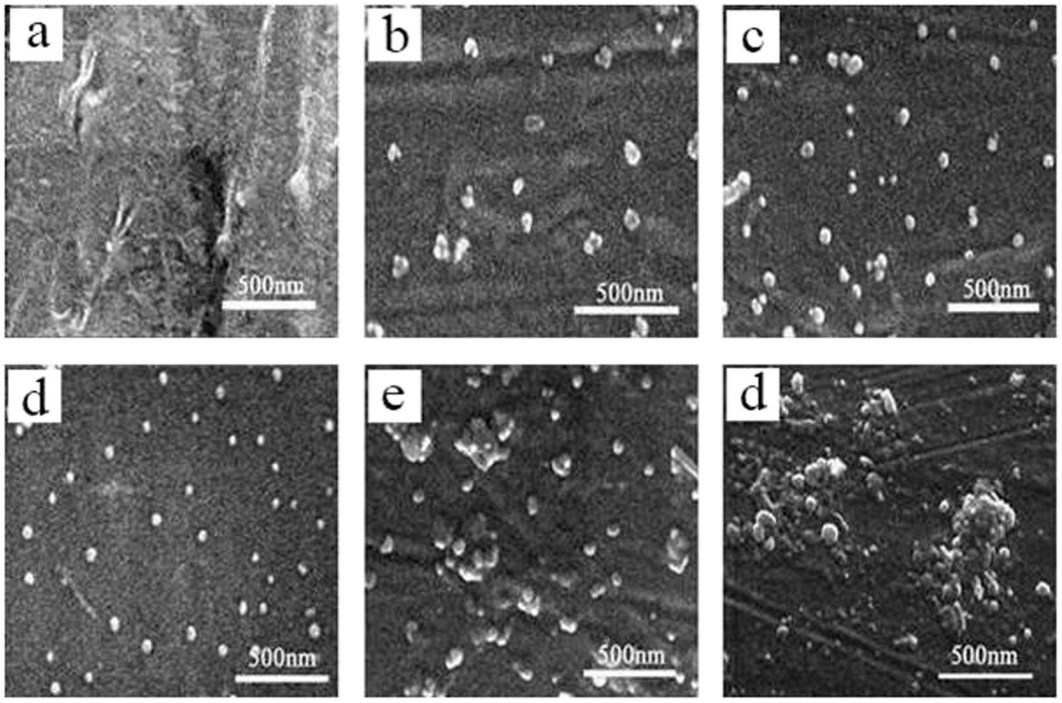

Figure 2. SEM micrographs of cryogenically fractured melt-processed PPS/C60 with different weight fractions of C_{60} (**a**) PPS; (**b**) 0.5 wt%; (**c**) 1 wt%; (**d**) 2 wt%; (**e**) 5 wt%; (**f**) 10 wt%.

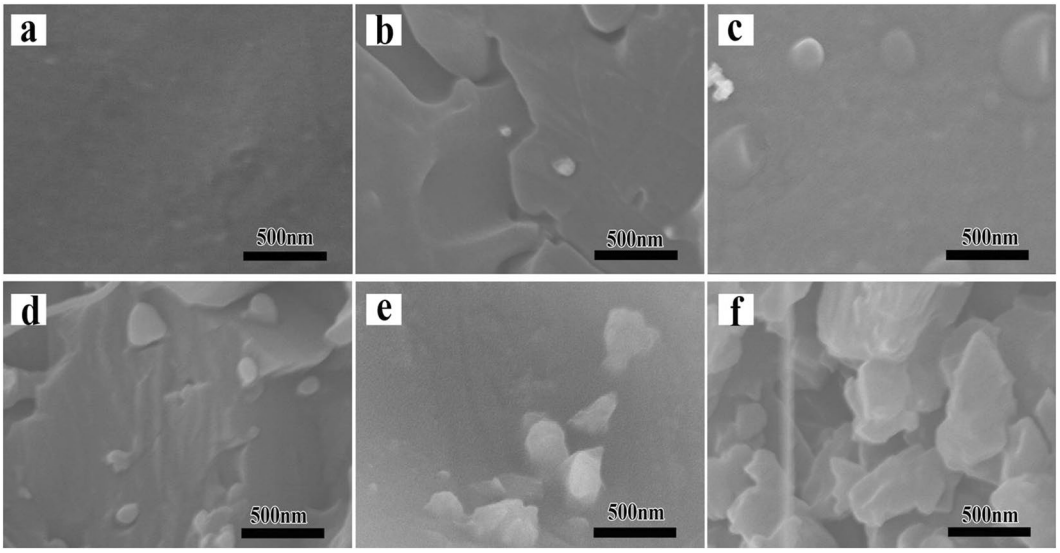

Figure 3. Cross-sectional SEM micrographs of cryogenically fractured melt-processed PPS/C_{60} with different weight fractions of C_{60} (**a**) PPS; (**b**) 0.5 wt%; (**c**) 1 wt%; (**d**) 2 wt%; (**e**) 5 wt%; (**f**) 10 wt%.

PPS molecular chain creeping and stretching in 1-chloronaphthalene, which effectively contributes to the well dispersion of C_{60} in PPS matrix. Although the alkylation or acylation was an effective functionalization method for fullerene[38,39], herein a C_{60}-thiol adducts by reacting C_{60} with the end group SH of PPS was easier to take place[32], and the covalent bond formation improved the C_{60}-matrix interfacial adhesion[6,7]. It is general known that the formation of π-π stacking interactions can be characterized through the shift of –CH bond. It is clear that the C-H bond absorption peaks of PPS located at 808.7 and 818.8 cm^{-1}. In PPS/C_{60} material, C-H vibration peak of PPS/C60 remain unchanged, which indicated that there only existed a weak π-π stacking interactions between C_{60} and PPS matrix[36,40].

In order to testify the existence of chain-extension reaction through the end-group reaction between PPS and C_{60}, PPS and PPS/C_{60} molecular weight were characterized by HTGPC (Table 1). As C_{60} content increased from 0.5 wt% to 2 wt%, PPS/C_{60} composite molecular weight propagated from 3.30×10^4 g·mol^{-1} to 4.19×10^4

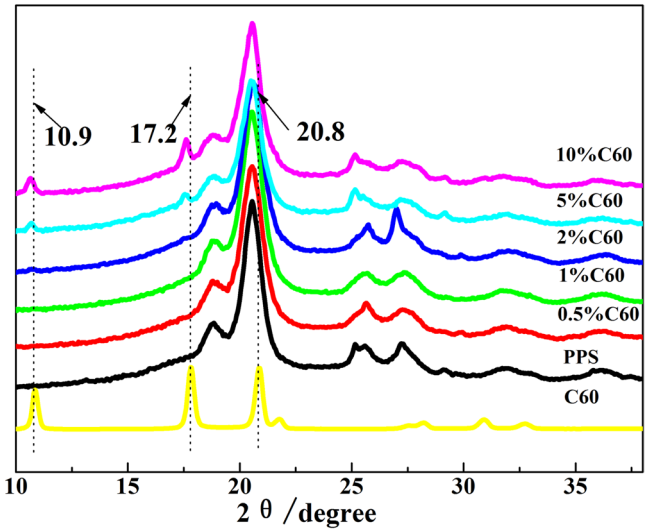

Figure 4. XRD spectra of C_{60}, PPS and PPS/C_{60} composite powder.

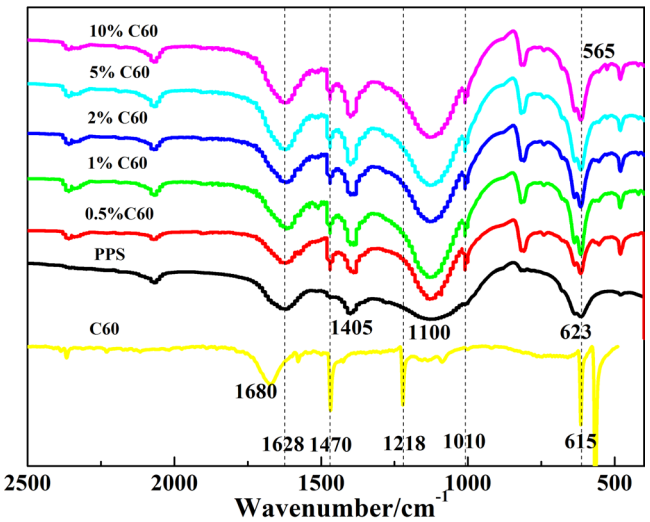

Figure 5. FT-IR spectra of C_{60}, PPS and PPS/C_{60} composite powder.

g·mol^{-1}, and polydispersity index (PDI) increased from 2.22 to 2.56. Only some PPS chains could interact with C_{60} to lead to the longer polymer chains. However, when C_{60} content reached 5 wt%, 5 wt% PPS/C_{60} composite molecular weight declined to 3.71×10^4 g·mol^{-1}. The deviation could be attributed to much more the low molecular weight C_{60} loading. A similar result was previously reported by Peng, K. J. & Liu, Y. L.[41]. HTGPC characterized results suggested some covalent bond formation between PPS and C_{60} through the C_{60}-thiol adducts and C_{60}-ArCl alkylation.

The crystallization and melting behavior of composites were investigated (Fig. 7), and the calorimetric parameters derived from non-isothermal DSC scans were listed in Table 2. As it can be observed, 0.5 wt% C_{60} had less influence on PPS crystallization temperature (Tc) increase (Fig. 7a), and 0.5 wt% PPS/C_{60} exhibited T_c of 217.2 °C with ΔH_c being 42.98 J/g. However, for 2 wt% PPS/C_{60}, T_c shifted to 227.6 °C with maximum ΔH_c being 48.23 J/g. AS for 5 wt% PPS/C_{60}, T_c increases to 223.8 °C with ΔH_c decline to 42.42 J/g. The further increase of C_{60} concentration in composites slowed the mobility and diffusion of PPS chains, which led to a significant decline of PPS crystallization temperature. Those behaviors observed are in agreement with that reported by Jeon *et al.*[42]. It was worthy of noting that 0.5 wt% PPS/C_{60} could not well act as heterogeneous nucleating agent to accelerate PPS nucleation, which suggested that the intense restrictions on chain mobility are imposed by the C_{60}–polymer chemical interactions.

T_m shifted gradually to higher temperature with increasing C_{60} content (See Fig. 7b and Table 2). 0.5 wt% PPS/C_{60} exhibited T_m of 275.1 °C with ΔHm being 41.50 J/g. As for 2 wt% PPS/C_{60}, T_m shifted to 277.3 °C with maximum ΔHm being 44.10 J/g. While for 5 wt% PPS/C_{60}, T_m increased to 282.4 °C with ΔHm decline to 40.14 J/g. In the case of 2 wt% PPS/C_{60}, both ΔH_m and ΔH_c achieve the maximum, and X_c reaches the maximum value 46.87%.

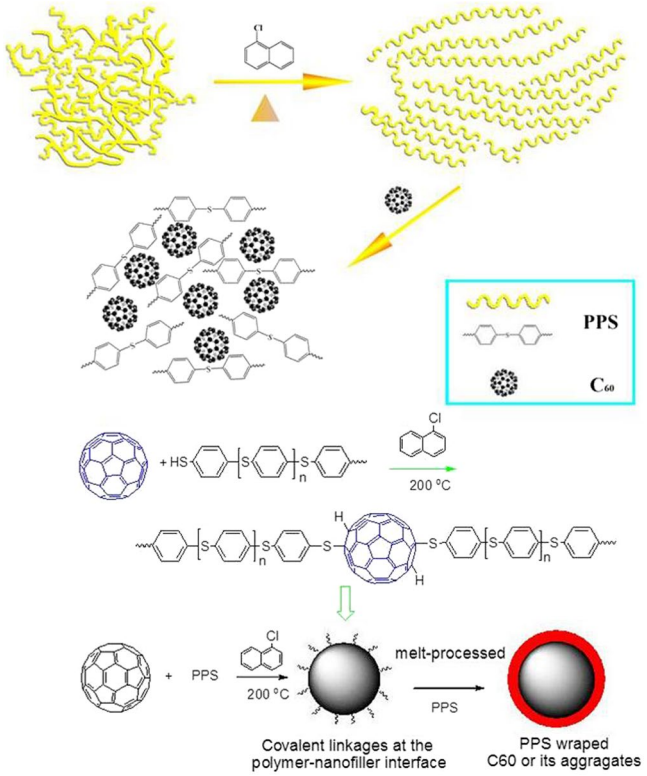

Figure 6. The chemical functionalization process of fullerenes and PPS/C_{60} interfacial adhesion changes during solution and melt processing.

Composites (wt%)	Mw (10^4 g·mol^{-1})	Mn (10^4 g·mol^{-1})	PDI
PPS	3.30	1.49	2.22
0.5	3.42	1.45	2.36
1	3.70	1.53	2.42
2	4.19	1.63	2.56
5	3.71	1.37	2.69
10	2.80	0.88	3.19

Table 1. Molecular weight and polydispersity index of different PPS.

The TG curves for the pure PPS matrix and composites under inert atmospheres were shown in Fig. 8, and their characteristic degradation parameters were summarized in Table 3. PPS displayed a single degradation stage that starts (T_i) at 502 °C and exhibited the maximum weight loss (T_{max}) rate at 541.3 °C. At 800 °C, the residual mass was about 52.2% of the initial weight. Clearly, the addition of 0.5–2 wt% C_{60} filler led to an improvement in the thermal stability of PPS matrix, and a maximum T_i increase (about 7 °C) was obtained at 2.0 wt% filler loading, and T_{max} increment for 2.0 wt% PPS/C_{60} was 5.5 °C. However, the significantly decline of T_i and T_{max} was detected at 10 wt% C_{60} loading, but the residual mass at 800 °C increased to 60.39% of the initial weight. Such results should be attributed to different factors. Firstly, C_{60} fillers are better dispersed within PPS matrix, which restricts chain mobility or diffusion to slow down the decomposition process[11]. Secondly, the covalent anchoring of PPS to C_{60} leads to a strong enhancement in the thermal conductivity that facilitates heat dissipation within the composite[43]. The reason for the thermal stability decline at 5 and 10 wt% C_{60} loading might be attributed to the appearance of C_{60} agglomerates.

Figure 9 shows single fiber morphology of each sample respectively. The characterized results suggested the diameter of fibers were 45.2 ± 0.8 μm, 40.5 ± 0.5 μm, 42.5 ± 1.0 μm, 64.3 ± 1.0 μm, 47.6 ± 1.0 μm and 87.2 ± 0.8 μm, respectively, changing with the content of C_{60}. The mechanical behavior of PPS/C_{60} fibers was investigated by single fiber strength tester technique which provides additional information about filler-matrix and filler-filler interactions. Figure 10 showed the breaking strength, breaking elongation and tensile modulus of PPS/C_{60} fiber. The results of mechanical property study indicated that the concentration of C_{60} had a greater influence on the mechanical performance of composites. As C_{60} nanofiller content increase, the breaking strength and tensile modulus of composites firstly increased and then decreased. When C_{60} concentration reached 2 wt%, the breaking

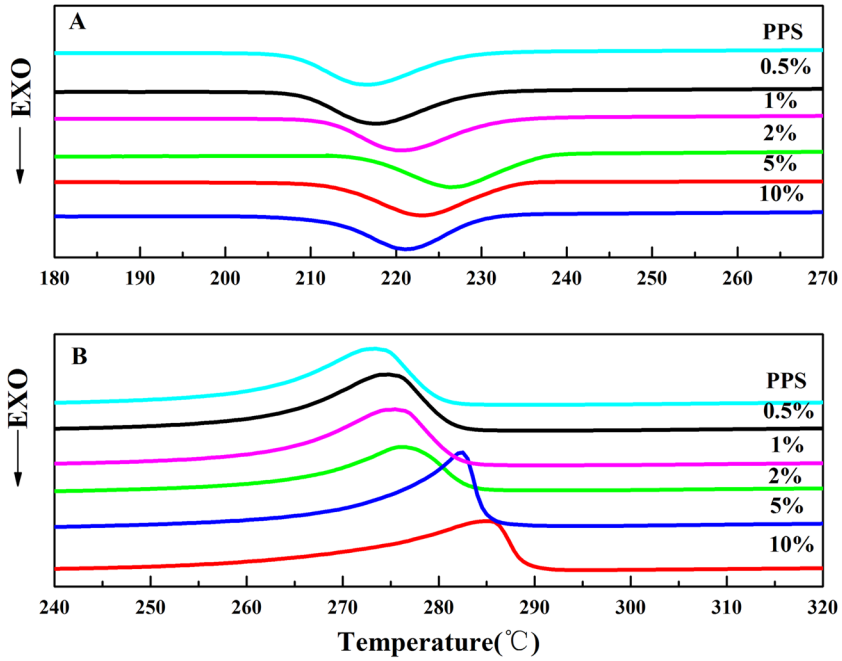

Figure 7. DSC thermograms obtained at a rate of 10 °C/min: (**a**) DSC cooling curves of PPS/C_{60}; (**b**) DSC heating curves of PPS/C_{60}.

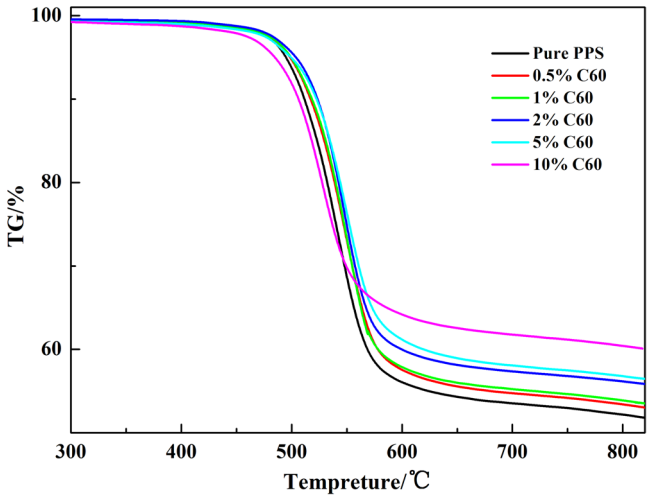

Figure 8. TG curves of PPS and PPS/C_{60}).

C_{60} content (wt%)	Tc (°C)	ΔH_c (J/g)	Tm (°C)	ΔH_m (J/g)	Xc (%)	ΔT (°C)
0	215.6	−49.11	272.5	43.43	46.77	38.7
0.5	217.2	−42.98	273.6	41.50	41.14	57.9
1	220.5	−44.22	275.6	42.10	42.54	55.6
2	227.6	−48.23	276.2	44.10	46.87	49.7
5	223.8	−42.42	282.4	40.14	44.89	61.7
10	221.7	−41.72	285.5	41.45	41.83	60.7

Table 2. DSC traces for PPS and PPS/C_{60}.

strength and tensile modulus of composites achieved maximum 290 MPa and 605 MPa, and those value were 7.72 and 11.2 times as that of pure PPS, respectively. The breaking elongation of PPS/C_{60} composites always decreased with increasing C_{60} content (Fig. 10b). The excellent mechanical properties of PPS/C_{60} were attributed to the

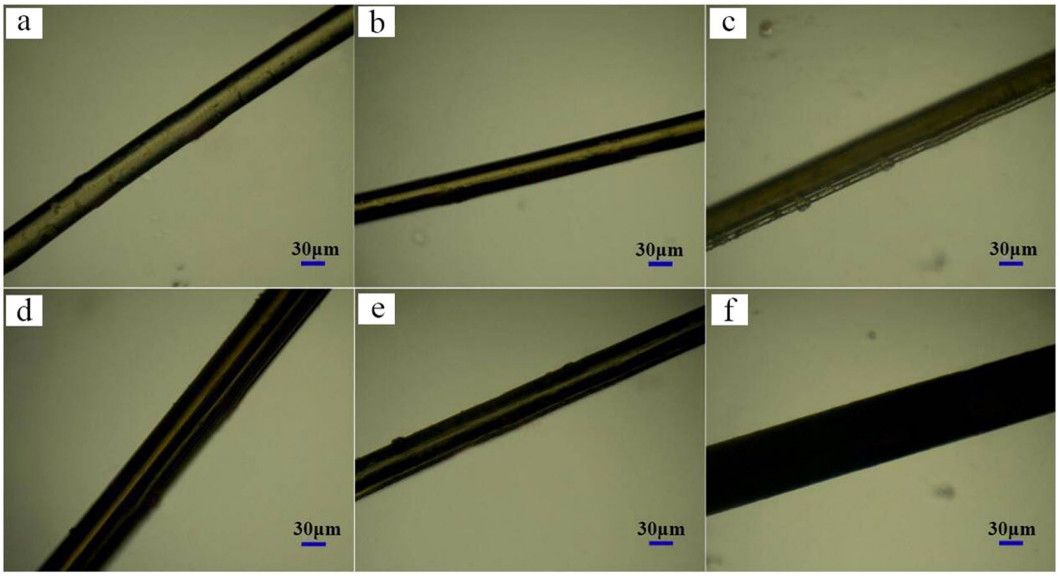

Figure 9. Micrographs of PPS/C_{60} with different weight fractions of C_{60} (**a**) PPS; (**b**) 0.5 wt%; (**c**) 1 wt%; (**d**) 2 wt%; (**e**) 5 wt%; (**f**) 10 wt%.

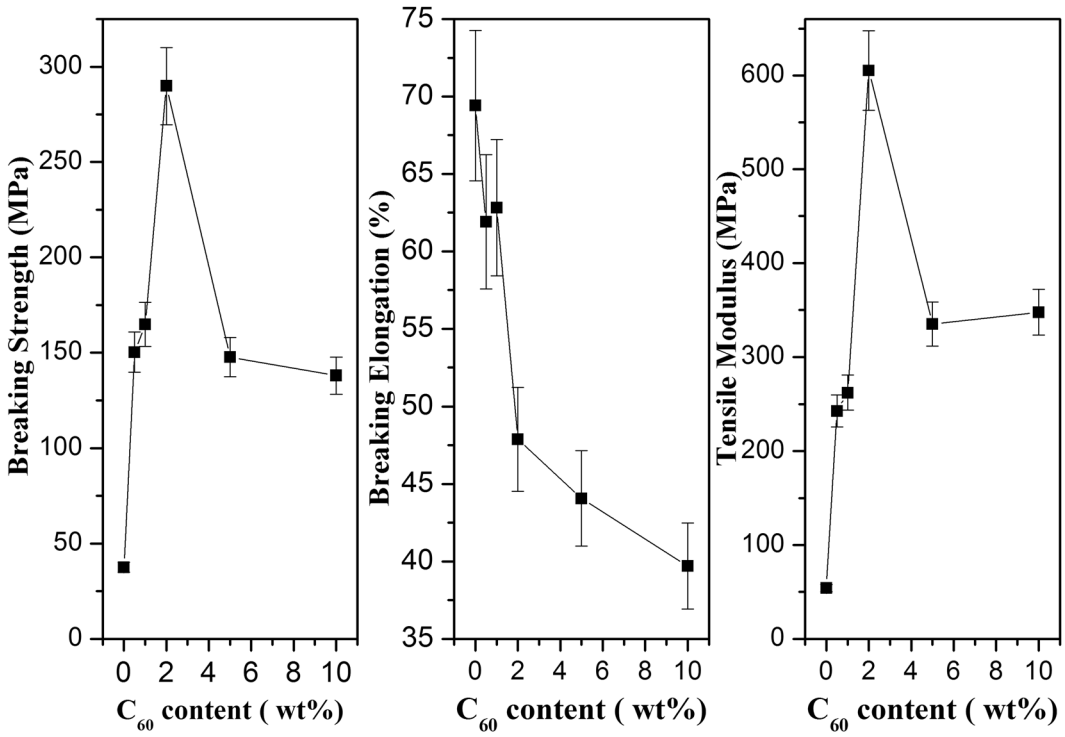

Figure 10. Mechanical properties of PPS/C_{60} fiber with different addition amount of C_{60}: (**a**) breaking strength; (**b**) breaking elongation; (**c**) tensile modulus.

heterogeneous nucleation of C_{60} during PPS crystallization, the formation of a large number of covalent bond by C_{60}-thiol adducts and π-π stacking interactions between C_{60} surface and PPS matrix. However, the excessive addition of C_{60} caused a significant reduction of breaking strength, e.g., the breaking strength of 10 wt% C_{60} composite declined to 148 MPa. The excessive addition of C_{60} reduced PPS crystallization degree and decreased the combination between PPS and C_{60}, which were attributed to the phenomenon of C_{60} aggregation. These results can also confirm by the SEM and TEM images of PPS/C_{60} composites presented in Figs 1–2.

PPS is an insulating material (σ 10^{-16} S/cm), which limits its use in self-health monitoring, electro-actuation, etc[32]. Herein, C_{60} was used as conductive fillers to improve PPS electrical conductivity and the electrical performance of PPS/C_{60} composites were compared (Fig. 11). As C_{60} nanofiller content increase, the electrical conductivity of

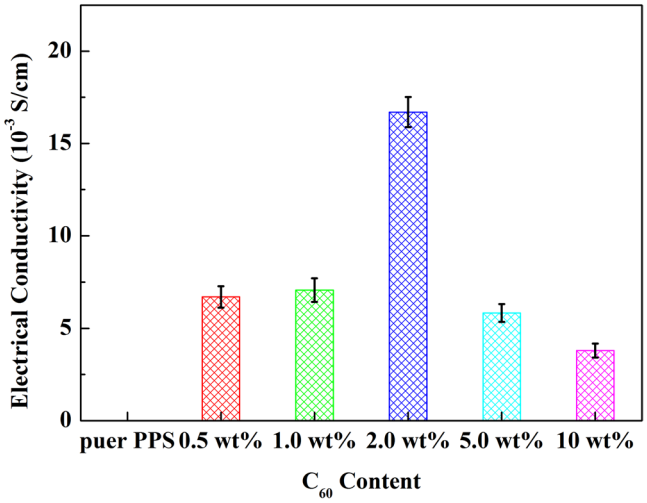

Figure 11. Room temperature electrical conductivity (r) of PPS/$_{C60}$ composites.

C_{60} content (wt%)	T_i (°C)	T_{max} (°C)	The residual mass at 800 °C (wt%)
0	502.0	541.3	52.16
0.5	506.4	546.3	52.37
1	507.2	546.6	53.78
2	509.0	546.8	56.21
5	505.5	544.0	56.79
10	497.6	534.0	60.39

Table 3. Thermogravimetric data under nitrogen atmosphere.

PPS/C_{60} composites firstly increased and then decreased. When C_{60} concentration reached 2 wt%, the electrical conductivity of composites achieved maximum 1.67×10^{-2}S/cm, much higher than the value of pure PPS. The excellent electrical conductivity of 2 wt% PPS/C_{60} composites was attributed to the well dispersed C_{60} fillers, and the maximum conductive networks might be formed in the composite at appropriate C_{60} content because of the conductive network formation[44]. C_{60} fillers are well dispersed in the PPS matrix owing to the covalent bond formation by main C_{60}-thiol adducts and mino C_{60}-ArCl alkylation between C_{60} surface and PPS. However, the excessive addition of C_{60} nanofillers caused a significant reduction of electrical conductivity, e.g., the electrical conductivity of 10 wt% C_{60} composite declined to 3.79×10^{-3}S/cm, due to the phenomenon of C_{60} aggregation.

Conclusions

PPS composites with well-dispersed C_{60} had been prepared by solution co-blending method because solvent promotes the tangled PPS molecular chains creeping and stretching. The electrical conductivity value of 2 wt% achieved the maximum, and the excellent electrical conductivity of 2 wt% PPS/C_{60} composites was mainly attributed to the covalent bond formation by main C_{60}-thiol adducts and minor C_{60}-ArCl alkylation between C_{60} surface and PPS, but C_{60} aggregation reduced composite electrical conductivity. Furthermore, 2 wt% C_{60} could effectively increase PPS crystalli zation temperature, thermal stability and mechanical performance. However, the excessive C_{60} loading reduced the PPS crystallization degree and caused C_{60} re-aggregation, which led to poorer mechanical performance of PPS/C_{60} composite.

References

1. Kroto, H. W., Heath, J. R., O'Brien, S. C., Curl, R. F. & Smalley, R. E. C60: Buckminsterfullerene. *Nature* **318**, 162–163 (1985).
2. Kratschmer, W., Lamb, L. D., Fostiropoulos, K. & Huffman, D. R. Solid C60: a new form of carbon. *Nature* **347**, 354–358 (1990).
3. Giacalone, F. & Martín, N. Fullerene polymers: Synthesis and properties. *Chem. Rev.* **106**, 5136–5190 (2006).
4. Lu, G., Li, L. & Yang, X. Creating a uniform distribution of fullerene C60 nanorods in a polymer matrix and its photovoltaic applications. *Small* **5**, 601–606 (2008).
5. Rajagopalan, M. & Oh, I. K. Fullerenol-Based Electroactive Artificial Muscles Utilizing Biocompatible Polyetherimide. *ACS Nano* **5**, 2248–2256 (2011).
6. Huang, X. D. & Goh, S. H. Interpolymer complexes through hydrophobic interactions: C-60-end-capped poly(ethylene oxide)/poly(methacrylic acid) complexes. *Macromolecules* **33**, 8894–8897 (2000).
7. Coro, J., Suárez, M., Silva, L. S. R., Eguiluz, K. I. B. & Salazar-Banda, G. R. Fullerene applications in fuel cells: A review. *Int. J. Hydrogen Energ.* **41**, 17944–17959 (2016).
8. Brady, D. G. Poly (Phenylene Sulfide)–How, when, why, where and where now. *Appl. Poly. Symp.* **36**, 231–239 (1981).
9. Frommer, J. E. Conducting polymer solutions. *Acc. Chem. Res.* **19**, 2–9 (1986).

10. Bo, Y., Long, C., Meifang, Z. & Yanmo, C. Reactive blends of poly(phenylene sulfide)/hyperbranched poly(phenylene sulfide). *Macromol. Symp.* **254**, 167–172 (2007).
11. Diez-Pascual, A. M. & Naffakh, M. Enhancing the thermomechanical behaviour of poly(phenylene sulphide) based composites via incorporation of covalently grafted carbon nanotubes. *Compos. A* **54**, 10–19 (2013).
12. Spitalsky, Z., Tasisb, D., Papagelis, K. & Galiotis, C. Carbon nanotube-polymer composites: Chemistry, processing, mechanical and electrical properties. *Prog. Polym. Sci.* **35**, 357–401 (2010).
13. Díez-Pascual, A. M. & Naffakh, M. Tuning the properties of carbon fiber-reinforced poly(phenylene sulphide) laminates via incorporation of inorganic nanoparticles. *Polym* **53**, 2369–2378 (2012).
14. Díez-Pascual, A. M., Naffakh, M., Marco, C. & Ellis, G. Mechanical and electrical properties of carbon nanotube/poly(phenylene sulphide) composites incorporating polyetherimide and inorganic fullerene-like nanoparticles. *Compos. A* **43**, 603–612 (2012).
15. Naffakh, M., Díez-Pascual, A. M., Marco, C. & Ellis, G. J. Morphology and thermal properties of novel poly(phenylene sulfide) hybrid nanocomposites based on single-walled carbon nanotubes and inorganic fullerene-like WS2 nanoparticles. *Mater. Chem.* **22**, 1418–1425 (2012).
16. Díez-Pascual, A. M., Naffakh, M., Marco, C. & Ellis, G. Rheological and Tribological Properties of Carbon Nanotube/Thermoplastic Nanocomposites Incorporating Inorganic Fullerene-Like WS2 Nanoparticles. *J. Phys. Chem. B* **116**, 7959–7969 (2012).
17. Díez-Pascual, A. M. & Naffakh, M. Grafting of an aminated poly(phenylene sulphide) derivative to functionalized single-walled carbon nanotubes. *Carbon* **50**, 857–868 (2012).
18. Díez-Pascual, A. M. & Naffakh, M. Towards the development of poly(phenylene sulphide) based nanocomposites with enhanced mechanical, electrical and tribological properties. *Mater. Chem. Phys.* **135**, 348–357 (2012).
19. Gonzalez-Domınguez, J. M. *et al*. Covalent functionalization of MWCNTs with poly(p-phenylene sulphide) oligomers: a route to the efficient integration through a chemical approach. *J. Mater. Chem.* **22**, 21285–21297 (2012).
20. In-Yup, J., Hwa-Jeong, L., Yeong, S. C., Loon-Seng, T. & Jong-Beom, B. Semimetallic Transport in Nanocomposites Derived from Grafting of Linear and Hyperbranched Poly(phenylene sulfide)s onto the Surface of Functionalized Multi-Walled Carbon Nanotubes. *Macromolecules* **41**, 7423–7432 (2008).
21. Bahadur, S. & Sunkara, C. Effect of transfer film structure, composition and bonding on the tribological behavior of polyphenylene sulfide filled with nano particles of TiO2, ZnO, CuO and SiC. *Wear* **258**, 1411–1421 (2005).
22. Schwartz, C. J. & Bahadur, S. Studies on the tribological behavior and transfer film–counterface bond strength for polyphenylene sulfide filled with nanoscale alumina particles. *Wear* **237**, 261–273 (2000).
23. Zhao, Y. F., Xiao, M., Wang, S. J., Ge, X. C. & Meng, Y. Z. Preparation and properties of electrically conductive PPS/expanded graphite nanocomposites. *Compos. Sci. Technol.* **67**, 2528–2534 (2007).
24. Shingankuli, V. L., Jog, J. P. & Nadkarni, V. M. Thermal and crystallization behavior of engineering polyblends I Glass reinforced polyphenylene sulfide with polyethylene terephthalate. *J. Appl. Polym. Sci.* **36**, 335–351 (1988).
25. Lee, I. H., Han, S. W. & Cho, H. J. Nanoparticle-directed crystallization of calcium carbonate. *Adv. Mater.* **13**, 1617–1620 (2001).
26. Lu, D. & Pan, S. W. Effects of ball milling dispersion of nano-SiOx particles on impact strength and crystallization behavior of nano-SiOx-poly (polyphenylene sulfide) nanocomposites. *Polym. Eng.* **46**, 820–825 (2006).
27. Cho, M. H. & Bahadur, S. A. Study of the thermal, dyamic mechanical and tribological properties of polyphenylene sulfide composites reinforced with carbon nanofibers. *Tribol. Lett.* **25**, 237–245 (2007).
28. Yu, S., Wong, W. M., Hu, S. & Juay, Y. K. The characteristics of carbon nanotube reinforced poly(phenylene sulphide) nanocomposites. *J. Appl. Polym. Sci.* **113**, 3477–3483 (2009).
29. Yang, J. *et al*. Preparation and properties of poly(pphenylene sulphide)/multiwall carbon nanotube composites obtained by melt compounding. *Compos. Sci. Technol.* **69**, 147–153 (2009).
30. Tabor, B., Magre, E. P. & Boon, J. Crystal structure of poly (p-phenylene sulfide). *Eur. Poly. J.* **7**, 1127–1133 (1971).
31. Li, B., Tao, X. T., Kasai, H., Oikawa, H. & Nakanishi, H. Size control for fullerene C-60 nanocrystals during the high temperature and high pressure fluid crystallization process. *Mater. Lett.* **61**, 1738–1741 (2007).
32. Zhang, T. *et al*. Synthesis, properties of fullerene-containing polyurethane-urea and its optical limiting absorption. *Polym* **44**, 2647–2654 (2003).
33. Díez-Pascual, A. M. *et al*. Grafting of a hydroxylated poly(ether ether ketone) to the surface of single-walled carbon nanotubes. *J. Mater. Chem.* **38**, 8285–8296 (2010).
34. Jeon, I. J., Tan, L. S. & Baek, J. B. Nanocomposites derived from *in situ* grafting of linear and hyperbranched poly(ether-ketone)s containing flexible oxyethylene spacers onto the surface of multiwalled carbon nanotubes. *J. Polym. Sci. A. Polym. Chem.* **46**, 3471–3481 (2008).
35. Zimmerman, D. A., Koenig, J. L. & Ishida, H. Infrared and Raman spectroscopy of cyclohexa(p-phenylene sulfide) and the polymer obtained therefrom. *Polym.* **40**, 4723–4731 (1999).
36. Zhang, M. L., Wang, H. X., Li, Z. H. & Cheng, B. W. Exfoliated graphite as a filler to improve poly(phenylene sulfide) electrical conductivity and mechanical properties. *RSC Adv.* **5**, 13840–13849 (2015).
37. Zimmerman, D. A., Koenig, J. L. & Ishida, H. *Polymerization of poly (p-phenylene sulfide) from a cyclic precursor. Polymer* **40**, 4723–4731 (1999).
38. Hayashi, S., Yorimitsu, H. & Oshima, K. Synthesis of Epoxides by Palladium-Catalyzed Reactions of Tertiary Allyl Alcohols with Aryl or Alkenyl Halides. *J. Am. Chem. Soc.* **131**, 2052–2053 (2009).
39. Lu, S., Si, W. L., Bao, M., Yamamoto, Y. & Jin, T. Co-Catalyzed Radical Cycloaddition of [60] Fullerene with Active Dibromides: Selective Synthesis of Carbocycle-Fused Fullerene Monoadducts. *Org. Lett.* **15**, 4030–4033 (2013).
40. Zhang, M. L. *et al*. Effects of hydrogen bonding between MWCNT and PPS on the properties of PPS/MWCNT composites. *RSC Adv.* **6**, 92378–92386 (2016).
41. Peng, K. J. & Liu, Y. L. Preparation and toroid formation of multiblock polystyrene/C60 nanohybrids. *Macromolecules* **44**, 5006–5012 (2011).
42. Jeon, I. Y., Lee, H. J., Choi, J. S., Tan, L. S. & Baek, J. B. Semimetallic Transport In Nanocomposites Derived from Grafting of Linear and Hyperbranched Poly(phenylene sulfide)s onto the Surface of Functionalized Multi-Walled Carbon Nanotubes. *Macromolecules* **41**, 7423–7432 (2008).
43. Shenogin, S., Bodapati, A., Xue, L., Ozisik, R. & Keblinski, P. Effect of chemical functionalization on thermal transport of carbon nanotube composites. *Appl. Phys. Lett.* **85**, 2229–2231 (2004).
44. Li, C. Y., Li, Z. H., Cao, L. & Cheng, B. W. Graphene preparation by phenylmagnesium bromide and its excellent electrical conductivity performance in Graphene/Poly(p-phenylene sulfide) composites. *Ind. Eng. Chem. Res.* **55**, 10860–10867 (2016).

Acknowledgements

The authors are grateful for the financial support from National Natural Science Foundation of China (Nos 51603145 and 21376177) and Tianjin Natural Science Foundation of China (nos. 15JCZDJC7000). This work is also supported by China National Textile and Apparel Council (J201406) and China Petroleum Chemical Co Technology Development Project (208068, 201100, 215038 and 216090).

Author Contributions

M.Z., X.W., B.C. and Z.L. have contributed to the design of the study and the critical revision of the article. M.Z. Y.B. and Z.L. did the experiments, analyzed the data, prepared Figures and drafted the article.

Additional Information

Competing Interests: The authors declare that they have no competing interests.

Publisher's note: Springer Nature remains neutral with regard to jurisdictional claims in published maps and institutional affiliations.